Acta Materialia 221 (2021) 117386

Contents lists available at ScienceDirect

Acta Materialia

journal homepage: www.elsevier.com/locate/actamat

Full length article

Investigation of self-heating and dissipative effects in ferroelectric ceramics subjected to compressive mechanical cyclic loading

Mahmoud Barati[a,b,c,*], Behnaz Amini[c], Valentin Segouin[a,b], Laurent Daniel[a,b], Shabnam Arbab Chirani[c], Sylvain Calloch[d]

[a] Université Paris-Saclay, Centrale Supélec, CNRS, Laboratoire de Génie Electrique et Electronique de Paris, 91192 Gif-sur-Yvette, France
[b] Sorbonne Université, CNRS, Laboratoire de Génie Electrique et Electronique de Paris, 75252 Paris, France
[c] Ecole Nationale d'Ingénieurs de Brest, ENIB, UMR CNRS 6027, IRDL, F-29200 Brest, France
[d] Ecole Nationale Supérieure de Techniques Avancées Bretagne, ENSTA Bretagne, UMR CNRS 6027, IRDL, F-29200 Brest, France

ARTICLE INFO

Article history:
Received 27 May 2021
Revised 31 August 2021
Accepted 5 October 2021
Available online 9 October 2021

Keywords:
PZT ferroelectric ceramic
Mechanical cyclic loading
Dissipation energy
Self-heating measurements
Infrared thermography
Digital image correlation

ABSTRACT

In this study the behavior of a soft PZT ceramic subjected to compressive cyclic loadings is investigated with the aim of providing an insight into different dissipative processes which affect the ferroelastic cyclic behavior of the material. Two quantitative imaging techniques, infrared (IR) thermography and digital image correlation (DIC), are employed to measure superficial temperature and in-plane displacement of the sample under mechanical cyclic loadings. Thermal and strain responses are further deduced from these measurements. This allows to quantify the energy dissipated by the material during applied mechanical loadings. Self-heating (SH) and DIC measurements reveal that, even in the piezoelectric regime, the level of dissipation is significant. This suggests that PZT ceramic response under cyclic compression is significantly influenced by domain switching mechanisms. The two imaging techniques are shown to be efficient tools to identify domain wall activity in ferroelectric ceramics and can be advantageously substituted for polarization measurements when polarization variations are too small to be detected. It is also shown that, due to the initial compressive stress experienced by all specimens, the domain wall activity under cyclic uniaxial compressive stress is almost independent of the initial polarization state of the material.

1. Introduction

Perovskite-type ferroelectrics such as Lead Zirconate Titanate (PZT) are being extensively used in electromechanical devices such as actuators or sensors [1]. The key feature used in these devices is the strong electromechanical coupling effects exhibited by the ferroelectric ceramics. In most of these systems, ferroelectric materials work under cyclic electromechanical loadings. The cyclic loading is associated to energy dissipation, that may induce material degradation. The degradation of the material properties during cyclic loadings raises concerns and challenges since it significantly limits the use of these materials [2]. Thereby, to fully exploit the potential applications of ferroelectric materials, investigations on dissipation sources are critically important, eventually leading to a better understanding of different dissipation and degradation mechanisms.

In ferroelectric materials, intrinsic and extrinsic effects play a major role on polarization and strain changes under electrical/mechanical loadings [3–5]. Intrinsic effects refer to elastic, dielectric and piezoelectric behaviors associated to changes in strain and polarization occurring at the crystal lattice scale. Extrinsic effects refer to ferroelastic and ferroelectric behaviors associated to 180 ° and/or non-180 ° domain wall motions. It is worth noting that 180 ° domain wall motions do not contribute to the change in macroscopic strain [6,7]. When an initially unpoled material is subjected to a sufficiently high electric field, it reaches a saturation polarization state. After removing the electric field, a large part of the polarization remains. When the material is reloaded - at small amplitude - around this remanent polarization state, its behavior is approximately linear and reversible as a function of electric field and stress. It is referred to as the piezoelectric regime [8]. Similar observations can be made with the application of stress; after a first application of a high amplitude stress, the macroscopic behav-

* Corresponding author at: Université Paris-Saclay, CentraleSupélec, CNRS, Laboratoire de Génie Electrique et Electronique de Paris, 91192 Gif-sur-Yvette, France.
E-mail address: mahmoud.barati@centralesupelec.fr (M. Barati).

https://doi.org/10.1016/j.actamat.2021.117386

ior appears approximately linear and reversible. The piezoelectric regime is the operating range of most practical applications. It is well known, however, that this linearity and reversibility are only apparent and that non-linear and dissipative mechanisms remain active [9].

Both intrinsic and extrinsic effects can contribute to the total energy dissipation [3,4,10,11]. The contribution of intrinsic effects appears at high frequency regime, mostly through damping and resonance effects [11]. They will not be considered in this study restricted to low frequency range (below 1 kHz). On the other hand, extrinsic contributions contribute to the dissipation through domain wall motions, domain switching and interaction between moving domain walls and defects [12,13]. Hence, the complexity of the mechanisms involved makes the identification and quantification of the different dissipation sources upon electromechanical cyclic loadings very challenging. Up to date, the complex energy dissipation behavior in ferroelectric materials is far from being fully understood, notably in perovskite materials with high electromechanical coupling factors, such as soft PZT ceramics [11].

For a thorough understanding of the energy dissipation mechanisms in ferroelectric materials, it is of paramount importance to separately investigate each dissipative mechanism. However, to the authors' knowledge, few works have been directed toward individually studying energy dissipation mechanisms [14]. Recognition of dissipative mechanisms during purely mechanical and purely electrical cyclic loadings can help understand dissipative mechanisms during complex electromechanical cyclic loadings. The influence of cyclic unipolar [15–20], sesquipolar [21–23] and bipolar [24–33] electric fields on the degradation of ferroelectric behavior has been investigated in great detail, whereas dissipative mechanisms and degradation processes during cyclic mechanical loading (i.e., ferroelastic behavior) have not received as much attention [34–37].

Multiple dissipative mechanisms occur at disparate scales (micro and/or nanoscale), and by common experimental setup, only the combined effects at macroscopic scale can be observed. Inadequacy (or inability) of exhibiting underlying micro/nanoscale processes in macroscopic parameters is most pronounced in cases where the macroscopic behavior of the material can be considered as a linear reversible approximation (i.e., piezoelectric regime). However, irreversible nonlinear processes still occur at micro/nanoscale levels [9], such as domain switching [38,39]. In this context, the implementation and development of full-field techniques represent an opportunity to collect high precision measurements in order to investigate the internal dissipative mechanisms in ferroelectrics. Two quantitative imaging techniques, infrared (IR) thermography and digital image correlation (DIC), can efficiently be used to characterize the material response under cyclic loadings. These methods give access to full-field measurements of temperature and strain fields.

IR thermography is a non-contact technique used for temperature-evolution measurements. The technique is generally employed to record the superficial temperature variations of a material under external load stimulation using an infrared camera. This technique indirectly provides information (both qualitative and quantitative) about the possible heat-dissipation mechanisms and can be used to establish the correlation between temperature evolution and corresponding heat-dissipation quantity. The temperature evolution of materials submitted to cyclic loading is linked to internal heat sources of different natures and to both time and spatial changes caused by conduction inside the material and heat transfer at the boundaries. During cyclic loading, the dissipated energy is converted into heat resulting in an increase in the specimen's mean temperature. In the first few cycles, the specimen's temperature rises abruptly, then in later cycling, it stabilizes or it keeps increasing with a milder slope. Provided that there is no external source, the temperature evolution during cyclic loading is called the material self-heating (SH). The temperature evolution can be detected by IR thermography technique as a function of time. Owing to the relevance of a link between material self-heating and irreversible processes (i.e., dissipative mechanisms), this method has been employed as a precious tool for several purposes, such as studying electric-field induced fatigue crack growth [40] or estimating the endurance limit of metallic materials [41,42], shape memory alloys [43,44] and composites [45,46]. However, as far as we are aware of, in the case of ferroelastic loading, no published studies have tried to use the self-heating approach as a framework to explain the relationship between dissipative mechanisms and thermal processes.

Digital image correlation (DIC) is a non-contact optical technique that can measure full-field strains at the surface of a sample. This technique can also indirectly provide insight into polarization and deformation mechanisms [47]. It was previously shown that, in the case of ferroelectric materials, DIC method can provide access to electric-induced strains down to 3×10^{-6} (standard deviation on the average value) and permits determining piezoelectric coefficients of the order of 20 pm/V and above [47–49]. Furthermore, previous studies showed that DIC-based strain field measurements can help to distinguish the contribution of isochoric mechanisms (i.e., domain switching) from non-isochoric mechanisms (e.g., piezoelectricity or crystal phase transition) [47–54]. Consequently, DIC-based investigation provides more insight about underlying microscale processes.

The electrocaloric effect and self-heating behavior stemming from dissipative phenomena have been extensively tackled in ferroelectric ceramics under electrical loadings [55–63]. By contrast, dissipative phenomena under mechanical loading (i.e., ferroelastic behavior) is hardly investigated [64]. In the present work, special attention is devoted to the investigation of dissipative phenomena during mechanical loading in soft PZT ceramic. The aim of this study is to contribute towards a better understanding of irreversible electromechanical phenomena in ferroelastic behavior. Irreversibility and energy dissipation processes under compressive mechanical cyclic loadings are quantitatively studied, and possible dissipative mechanisms are discussed. In practice, thermal, mechanical and electrical fields are required for evaluating the energy dissipation processes in ferroelectric ceramics. In this study, IR thermography and DIC techniques are employed for measuring thermal and mechanical fields in order to characterize the dissipated energy. IR thermography technique provides thermal images relevant to the material self-heating, and the heat sources associated with the material cycling are directly evaluated using the heat diffusion equation. This methodology is based on the link between heating effects and irreversible dissipative mechanisms (i.e., domain switching) during mechanical cyclic loading. The DIC technique gives access to surface displacement and strain fields. The obtained results from both imaging techniques in conjunction with polarization variations will then be combined to assess energy dissipation processes.

The paper is organized as follows: In the next section, the experimental setups and corresponding procedures and the studied material will be outlined. In Section 3, the self-heating test procedure and underlying assumptions of the 0D approach will be explained and then corresponding results will be presented. In Section 4 the results obtained from DIC measurements will be brought and finally all results will be discussed in Section 5.

2. Experimental procedure and studied material

2.1. DIC measurements

The experimental setup used for DIC measurements is described in Fig. A.1 (see appendix for details). The setup was de-

signed to apply a compressive force (F_3) up to -10 kN and to measure transverse and longitudinal strain components (ε_{11} and ε_{33}, respectively) using DIC system. The compressive quasi-static force was applied by a Zwick/Roell030 tension/compression machine and was measured by $a \pm 10$ kN load sensor (KAP-TC, Angewandte System Technik), mounted between the machine loading frame and the upper fixture. The sample was placed between two fixtures, electrically isolated from the ground using alumina parts. The upper fixture contains a ball-joint and all bearing surfaces were grinded and have a flatness within ±4 µm.

The electric displacement (D_3) was measured from the lower electrode of the sample using the conditioner with an operational amplifier integrator circuit [65,66]. The integrating capacitor of 2 µF was utilized to measure D_3. A real-time DSpace hardware module with a maximum sampling frequency of 50 kHz was used to acquire and to record F_3 and D_3. The module was controlled from computer 1 (see Fig. A1.b in appendix) using a real-time Graphical User Interface (GUI) and F_3 and D_3 were monitored and recorded on this computer with MATLAB/Simulink associated to GUI (DSpace ControlDesk).

To measure in-plane strain field by DIC [48,49], a suitable speckle pattern was painted on a lateral face of the samples so as to track local displacements. Details concerning the deposition process are described in [48,49]. During experiments, the speckled face of the sample was imaged by means of a high resolution Ximea MD091MU-SY (14 bits monochrome) camera mounted on a Questar QM100 MKIII long distance microscope. This high-resolution camera can acquire 3380 × 2708 px size images at a maximum frame rate of 5 Hz. This optical system was placed at distance of ∼ 37 cm from the sample surface, which results in the aperture of f/7, the optical resolution of ∼ 5 μm and the spatial sampling of ∼1.2 µm/px (area of ∼3.2 × 4 mm). The sample lighting was provided by an LLS 3 LED light source (SCHOTT North America, Inc.) and oriented with an optical fiber.

The camera was triggered by the dSPACE module to synchronize the image acquisition with the applied mechanical force and the images were stored on Computer 2 (see Fig. A1.b in appendix). After acquiring images, the in-plane displacement and strain fields were obtained using a post-processing Digital Image Correlation program (CorreliRT3) [49,67]. A detailed description of the optical setup and the DIC program can be found in [49].

It is worth noting that the homogeneity of the strain field was confirmed (standard deviation is about 5% of the average value and no more than 8%) and only the averaged value of strain components was considered in this study. Furthermore, to avoid edge effects, the data close to the border of images was discarded since this data leads to discontinuity in the displacement field and consequently to an inhomogeneous strain [47,48].

2.2. Self-heating measurements

The general testing set up dedicated to self-heating tests is presented in Fig. A.2 (see appendix for details). In order to perform the self-heating measurement tests, stress-controlled cyclic compression tests were carried out at room temperature, by means of an INSTRON all-electric dynamic test instrument (ElectroPuls E10000, which is designed based on the linear motor technology) with the capacity of ± 10 kN. The cyclic tests were conducted with different stress ratio and a loading frequency (f_r) of 30 Hz. Compression test fixtures were designed to ensure uniform loading conditions, independent of applied load level, during mechanical cycling. The designed upper fixture contains a spherical joint, which controls the parallelism between two fixture faces, the alignment of the applied load and, therefore, the homogenously compressive loading without bending. It is of particular importance to ensure that the uniform boundary conditions are maintained upon loading, which was verified by DIC measurements.

During the self-heating test, IR thermography technique was utilized to measure and to record the temperature evolution on the specimen surface. A mid-wavelength range infrared (MWIR) detector INFRATEC IR8300 was used with a full frame rate of 350 Hz. The detector format (IR pixels) was a 512 × 640 array of detectors digitized on 14 bits and sensitive in the 2.0–5.7 μm spectral band with a 15 μm pitch (distance between two detectors) and a temperature resolution as low as 0.02 K. The device was equipped with a Stirling cooler. The focal length of the optical lens was 50 mm, and its transmissivity was 0.94. The measuring range of the camera was chosen between -10 °C and 60 °C, and the frequency acquisition and the integration time were set to 23 Hz and 1600 µs, respectively. Infrared images were analyzed by means of the IRBIS 3 commercial software. To limit the errors associated with emissivity of the surface, the surface of the specimen was covered with a very fine coating of a strongly emissive black paint.

Special attention was given to minimize the influence of the environment thermal perturbations on the measurements and to provide a relatively thermally insulated system. In doing so, the specimen was surrounded by a black painted paperboard box between the testing machine frame, leaving only a rectangle area (an inspection window) in front of it, facing the IR camera. Moreover, a thick dark blanket was used to thermally insulate the whole testing machine frame and the IR camera.

Since, upon mechanical cycling, dissipative sources in metallic materials are more pronounced than those in ceramics, heat generation in the designed metallic fixtures is more than that in the PZT sample. Therefore, during cyclic loading, the temperature of metallic fixtures raises more than that of the specimen. Hence, the heat transfer direction is from metallic fixtures to the PZT sample, which is undesirable for dissipative energy evaluation purposes. Ideally, the heat transfer direction should be from the specimen to fixtures, and the reverse heat transfer direction leads to temperature measurement interferences. Hence, a closed-loop water cooling system (Neslab RTE-101 refrigerated bath chiller circulator in conjunction with copper pipes (i.e., cooling collars)) was designed to control the temperature of metallic fixtures. This cooling system minimizes the fixtures temperature variations during testing and ensures the heat transfer direction from specimen to fixtures. It is worth noting that by considering a temperature difference of about 1–2 °C between the specimen and fixtures, the influence of temperature fixtures on the stabilized mean temperature of the specimen is negligible (see appendix for details).

Obtaining information about heat sources requires solving the heat diffusion equation [41], which will be detailed in the following section. For each loading level, this equation links what is measurable, the temperature, to a dissipation heat source, which is an internal quantity of the material. When internal mechanical dissipations (i.e., heat sources) are spatially homogeneous in the tested specimen, temperature changes are homogeneously distributed over the volume of the material and there is no temperature gradient, which could result in a simplified form of the heat-diffusion equation. It was observed that the measured temperature field is homogeneous throughout the specimen surface during applied mechanical cyclic loadings, which leads to a reduced form of the heat equation. Hence, it is assumed that the temperature field is also homogeneous throughout the whole specimen volume and a zero-dimensional (0D) approach is adopted [41] (i.e., thermal sources are spatially homogeneous in the specimen studied). Thus, the averaged value of the temperature field over the specimen surface can be considered as the specimen temperature ($T_{specimen}$). On the other hand, heat generation in the fixtures has a detrimental effect on evaluating the internal thermal dissipation of the specimen. Thus, to eliminate this effect and to obtain the specimen

Table 1
Noliac NCE55 piezoelectric (d_{33} and d_{31}) and dielectric (κ_{33}) coefficients, density (ρ) and specific heat capacity (c), according to the datasheet [71].

Parameter	d_{33} (m/V)	d_{31} (m/V)	κ_{33}/κ_0	ρ (kg/m^3)	c (J/kg°K)
Value	670×10^{-12}	-260×10^{-12}	5000	8000	420

temperature evolutions relevant only to the internal dissipation, the mean temperature of the fixtures ($T_{upper\ fixture}$ and $T_{lower\ fixture}$) should be subtracted from $T_{specimen}$ (at the beginning of the self-heating test, the difference between the temperatures of fixtures and specimen temperature is about 1 °C). Therefore, the temperature change (θ^{0D}) is given by

$$\theta^{0D} = T_{\text{specimen}} - \frac{T_{\text{upperfixture}} + T_{\text{lowerfixture}}}{2} \tag{1}$$

2.3. Studied material

The studied piezoelectric material in this work is a soft lead zirconate titanate (PZT) ceramic from Noliac Inc. with silver electrodes on two opposite specimen's surfaces (NCE55, Noliac). The dimension of specimens is $4 \times 4 \times 4$ mm^3 and its piezoelectric and dielectric coefficients, density and specific heat capacity are summarized in Table 1. First of all, the quasi-static uniaxial compressive loading was performed on polarized PZT specimen to study the ferroelastic behavior and to examine the effect of ferroelastic domain switching on the stress-strain curve. The obtained results are illustrated in Fig. 1. The polarized PZT exhibits the typical mechanical behavior of a ferroelastic material [68–70]. As can be seen in Fig. 1, the stress-strain curves show a visible non-linearity in loading part, which is due to non-180 ° ferroelastic domains switching. During domain switching process, the domains are aligned in orientation closest to the direction perpendicular to the compressive stress. The stress-strain curves in unloading part are "*almost reversible and linear*" (Fig. 1a and b) and the polarization remains almost constant (Fig. 1c). To interpret the effects of different type of cyclic loading cases, it is prominent to have the same initial state for all loading cases. Therefore, unloading part of the ferroelastic behavior will be used to investigate dissipative phenomena upon mechanical cyclic loadings. Consequently, prior to applying cyclic loading, all samples (both polarized and non-polarized) were subjected to quasi-static compression loading-unloading up to -400 MPa. In the case of DIC samples, this procedure was also preceded by a series of mechanical cycles (at maximum amplitude), in order to reach a stabilized behavior and overcome the slight drift observed during the first cycles. This latter step is unnecessary for self-heating measurements since the number of cycles performed is much higher than the number required for stabilization.

3. Self-heating tests under compressive cyclic loading

3.1. Self-heating test protocol

The principle of a self-heating test protocol is shown in Fig. 2. The self-heating tests are carried out by applying several series of compressive cyclic loadings (or loading blocks) with an increasing stress amplitude upon the same loading frequency ($f_r = 30\,Hz$, here). The choice of the frequency is made so that the internal dissipation leads to achieving temperatures high enough to be detected using IR thermal camera. The considered value of the frequency makes it possible to achieve a temperature rise ($\bar{\theta}^{0D}$) of about 0.4 °C at last loading block (i.e., $\sigma_{mean} = -210\,MPa$ and $\sigma_{amp} = 190\,MPa$).

During self-heating test, the temperature evolution of the specimen is recorded through thermal imaging, which is accomplished by using IR camera. For instance, temperature evolution during the loading block "n" (in Fig. 2a) is schematically shown in Fig. 2b. Each loading block consists of two stages. The first stage is the force-controlled loading step, in which the sample is subjected to 3000 compressive sinusoidal loading cycles (i.e., 3000 cycles per block). During this stage, the temperature of the specimen initially increases with the number of applied cycles and then reaches a steady state. This specified number of cycles ($N = 3000$ cycles/block) is considered so that before achieving 3000 cycles, the temperature of the specimen stabilizes. Temperature evolution during the loading stage (stage I) is shown in Fig. 2b, which contains two classical phenomena. The first is a global rise in temperature (blue curve in Fig. 2b), which is related to energy dissipation. The second is the oscillation around the previous curve, which is related to the thermo-elastic coupling effect (red curve in Fig. 2b). The second stage is a cooling step, during which the compressive cyclic loading is ceased to have almost the same initial condition from one loading block to another. In the cooling phase, the specimen cools down to the initial temperature (θ_i^{0D}). It is worth noting that the cooling step removes the probability of any carryover of the temperature from a previous loading block to the subsequent one. The temperature evolution recorded confirms that the specimen is thoroughly cooled down at the end of second stage and is ready for the next loading sequence. This protocol is repeated for each sequence of cyclic blocks and allows the temperature evolution to be correlated to the compressive stress.

The thermal data recorded during the self-heating tests are analyzed to correlate the superficial temperature of the specimen to the internal dissipation. Combining the local expression of the first and the second principles of thermodynamics and neglecting the convective terms of the material derivative lead to the local heat diffusion equation as follows [72]

$$\rho c\dot{T} - div(\vec{q}) = \Delta + r + \rho T \frac{\partial^2 \psi}{\partial T \partial \boldsymbol{\varepsilon}^{el}} : \dot{\varepsilon}^{el} + \rho T \frac{\partial^2 \psi}{\partial T \partial V_k} : \dot{V}_k = \rho c S_t \tag{2}$$

where T and $\boldsymbol{\varepsilon}^{el}$ are the temperature and the elastic part of the strain tensor, respectively, $V_k (k = 1, \ldots, n)$ represents the n internal state variables, introduced to describe the microstructural state, and ψ is the Helmholtz free energy. The involved terms in Eq. (2) have the following physical significance:

- $\rho c\dot{T}$ reflects the stored/released heat rate; in which c and ρ are the specific heat capacity (at constant pressure) and the density, respectively, and it is assumed that c and ρ are independent of the temperature T,
- $div(\vec{q})$ stands for the volume heat rate losses by conduction, where $\vec{q}$ is the heat flux vector,
- $\Delta = \boldsymbol{\sigma} : \dot{\varepsilon}^{nl} - A_k : \dot{V}_k$ is the internal dissipated energy, where $\boldsymbol{\sigma}$ is the Cauchy stress tensor, $\boldsymbol{\varepsilon}^{nl}$ is the nonlinear part of the strain tensor and A_k denotes a set of thermodynamic forces associated to a set of the internal variables V_k,
- r is the external heat supply, it is assumed that r is time-independent,
- $\rho T \frac{\partial^2 \psi}{\partial T \partial \boldsymbol{\varepsilon}^{el}} : \dot{\varepsilon}^{el} + \rho T \frac{\partial^2 \psi}{\partial T \partial V_k} : \dot{V}_k$ are the thermodynamic coupling sources (i.e., thermo-elastic and thermo-mechanical and/or

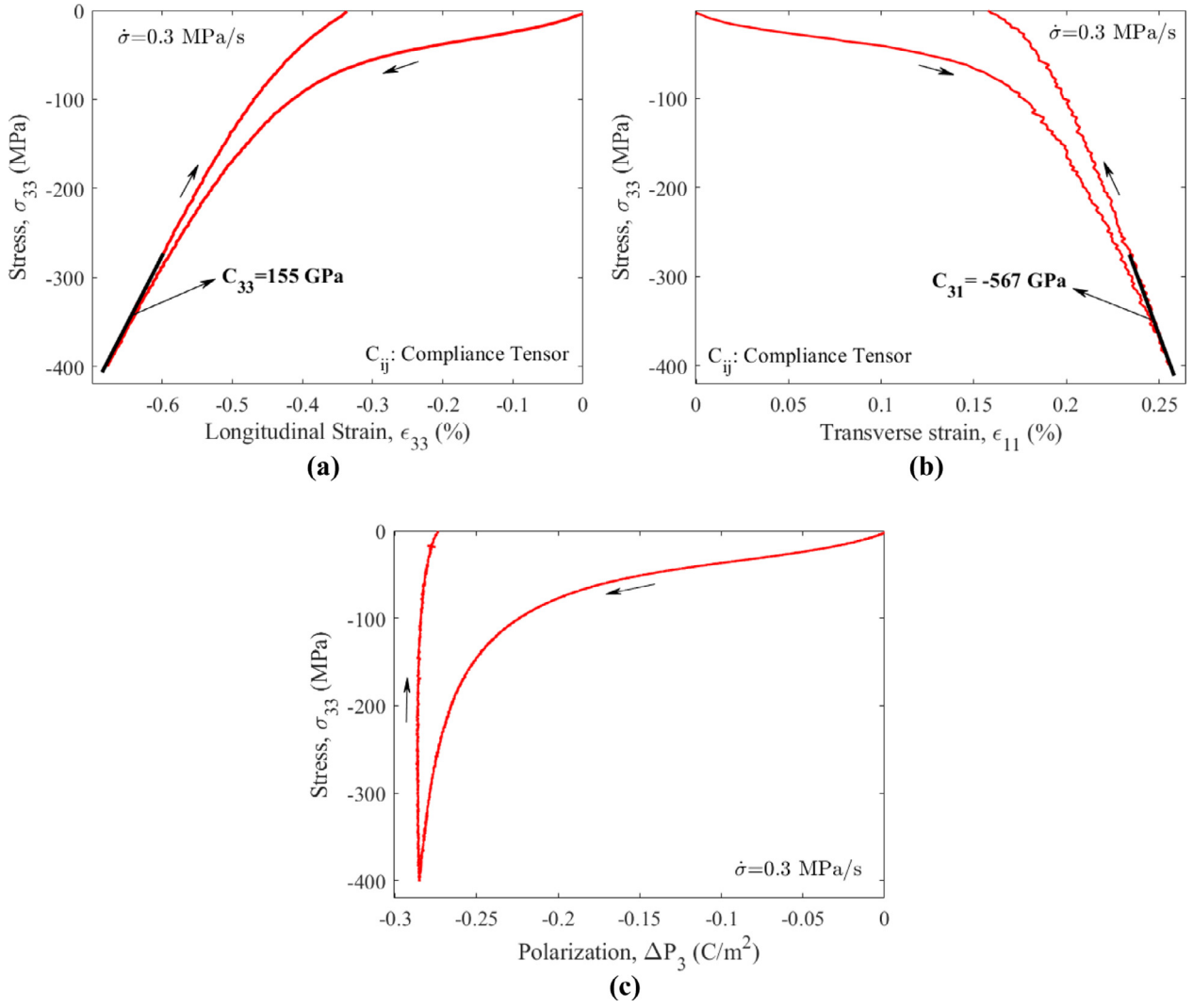

Fig. 1. Evolutions of (a) longitudinal and (b) transverse strains (obtained by DIC measurements) and (c) polarization variations upon quasi-static compression test performed on polarized PZT sample.

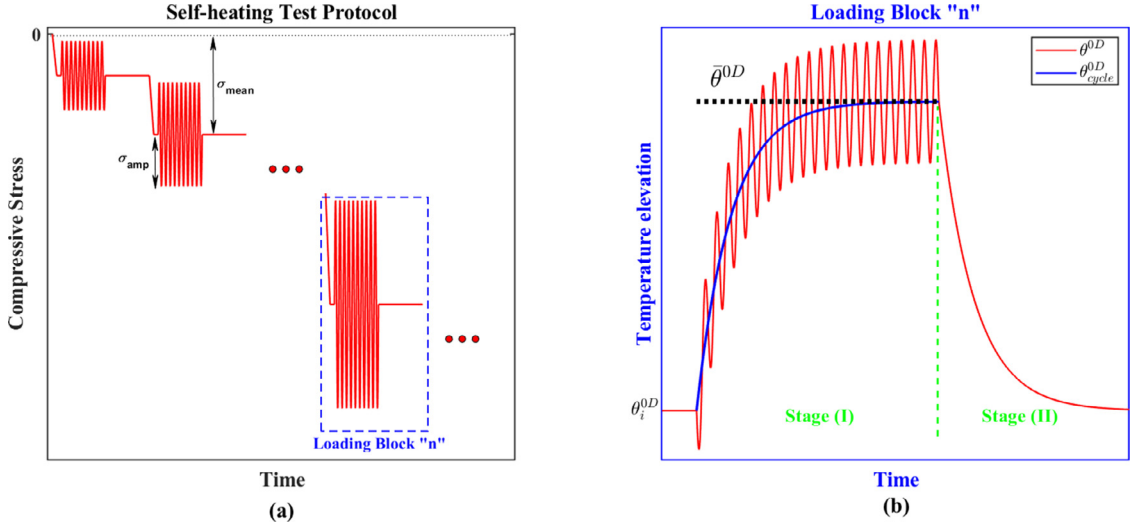

Fig. 2. (a) Schematic of successive series of compressive loading blocks (blocks 1, 2, and "*n*") in the self-heating test (b) Temperature elevation during loading block "*n*", θ^{0D} denotes the temperature elevation including fluctuations due to thermo-elastic coupling effect, while the mean temperature with no fluctuation is shown by θ^{0D}_{cycle}.

-electrical coupling sources), it is supposed that thermo-mechanical and thermo-electrical coupling sources are negligible and therefore the coupling terms are limited to the thermo-elastic source ($\rho T \frac{\partial^2 \psi}{\partial T \partial \boldsymbol{\varepsilon}^{el}} : \dot{\boldsymbol{\varepsilon}}^{el}$),
- $\rho c S_t$ is the local thermal source.

As evoked previously, by assuming a homogenous temperature field throughout the specimen volume, the 0D approach can be adopted [41] and the average temperature variation $\theta^{0D}(t)$ can be considered instead of the spatial temperature $T(x, y, z, t)$. It implies that the thermal sources are spatially homogeneous in the volume considered. Thus, by integrating Eq. (2) over the specimen volume, the heat equation reads [41]

$$\dot{\theta}^{0D}(t) + \frac{\theta^{0D}(t)}{\tau_{eq}^{0D}} = S_t^{0D}(t) \tag{3}$$

where S_t^{0D} is the average heat source throughout the specimen volume and τ_{eq}^{0D} is a time constant characterizing heat losses with the surroundings. The characteristic time depends on the dimensions and on the thermal conductivity of the specimen as well as on the heat transfer coefficients between the specimen and the fixtures and between the specimen and the surrounding environment.

It is worth noting that, by considering all above-mentioned assumptions, S_t^{0D}only consists of the internal dissipation and the thermo-elastic coupling term. The thermo-elastic coupling effect is a reversible phenomenon, and its variation vanishes at the end of each complete loading cycle (see Fig. 2b). Therefore, the integration of Eq. (3) over one cycle leads to

$$\dot{\theta}_{cycle}^{0D}(t) + \frac{\theta_{cycle}^{0D}(t)}{\tau_{eq}^{0D}} = \bar{S}_t^{0D} = f_r \int_{cycle} S_t^{0D} dt = \frac{f_r}{\rho c} \int_{cycle} \Delta dt = \frac{f_r \bar{\Delta}}{\rho c} \tag{4}$$

where θ_{cycle}^{0D} is the mean value of temperature evolution per cycle (see Fig. 2b). If the average value of the internal dissipation per cycle ($\bar{\Delta}$) is constant, as is shown in Fig. 2b, the mean temperature reaches a stabilized value ($\bar{\theta}^{0D}$) at the end of loading step of each block. It implies that the temperature rate is negligible at the end of loading step (i.e., $\dot{\theta}_{cycle}^{0D} \simeq 0$), and by virtue of Eq. (4), the internal dissipation corresponding to each stress amplitude (each loading block) can be obtained by

$$\bar{\Delta} = \frac{\rho c \bar{\theta}^{0D}}{f_r \tau_{eq}^{0D}} \tag{5}$$

To identify the characteristic time τ_{eq}^{0D}, in this study, the cooling part of self-heating data (second stage in Fig. 2b) is utilized. Eq. (6) is a solution of Eq. (4) during the cooling stage (when $\bar{S}_t^{0D} = 0$). Therefore, τ_{eq}^{0D} is estimated by fitting the cooling part of experimental data with Eq. (6) (i.e., the theoretical evolution of θ_{cycle}^{0D} during cooling step).

$$\theta_{cycle}^{0D} = \bar{\theta}_{cycle}^{0D} \times \exp\left(-t/\tau_{eq}^{0D}\right) \tag{6}$$

As an example, in Fig. 3, the results of the characteristic time identification are given for non-polarized PZT specimen over four loading blocks. It appears that the identified characteristic times are almost constant, and their slight discrepancies are attributed to the measurement noises.

3.2. Self-heating test results

In this section, the methodology developed in the previous section for evaluating the internal dissipation during self-heating tests is performed on polarized and non-polarized PZT specimens. As was mentioned in Section 2.3, prior to perform self-heating

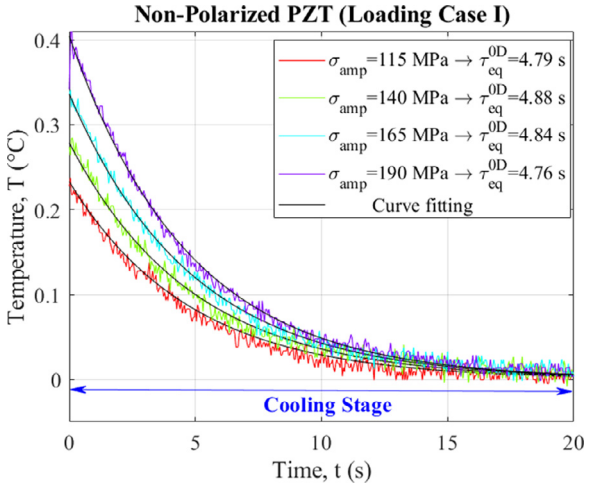

Fig. 3. Identification of characteristic time (τ_{eq}^{0D}(s)) by considering the cooling phase of the temperature evolution curves.

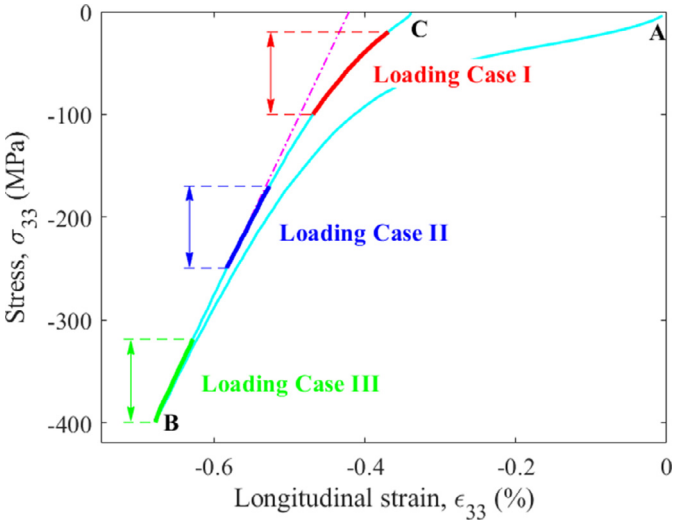

Fig. 4. First loading block of different loading cases considered for realizing self-heating tests.

tests, all samples (both polarized and non-polarized ones) were subjected to quasi-static compression loading-unloading up to -400 MPa (Fig. 4). In doing so, the unloading part of stress-strain curve (i.e., part B,C in Fig. 4) is used to ensure apparent macroscopic reversibility of the ferroelastic behavior with the aim of investigation of the internal dissipation upon compressive mechanical cyclic loadings.

Accordingly, in this study, three loading cases are considered to realize self-heating tests:

- Loading case I: maximum applied compressive stress is kept constant during all loading blocks and its value is equal to -20 MPa
- Loading case II: mean applied compressive stress is kept constant during all loading blocks and its value is equal to -210 MPa
- Loading case III: minimum applied compressive stress is kept constant during all loading blocks and its value is equal to -400 MPa

All self-heating tests comprise seven loading blocks with stress amplitudes of 40, 65, 90, 115, 140, 165, and 190 MPa. Thus, the stress range in the last loading block is the same for all loading

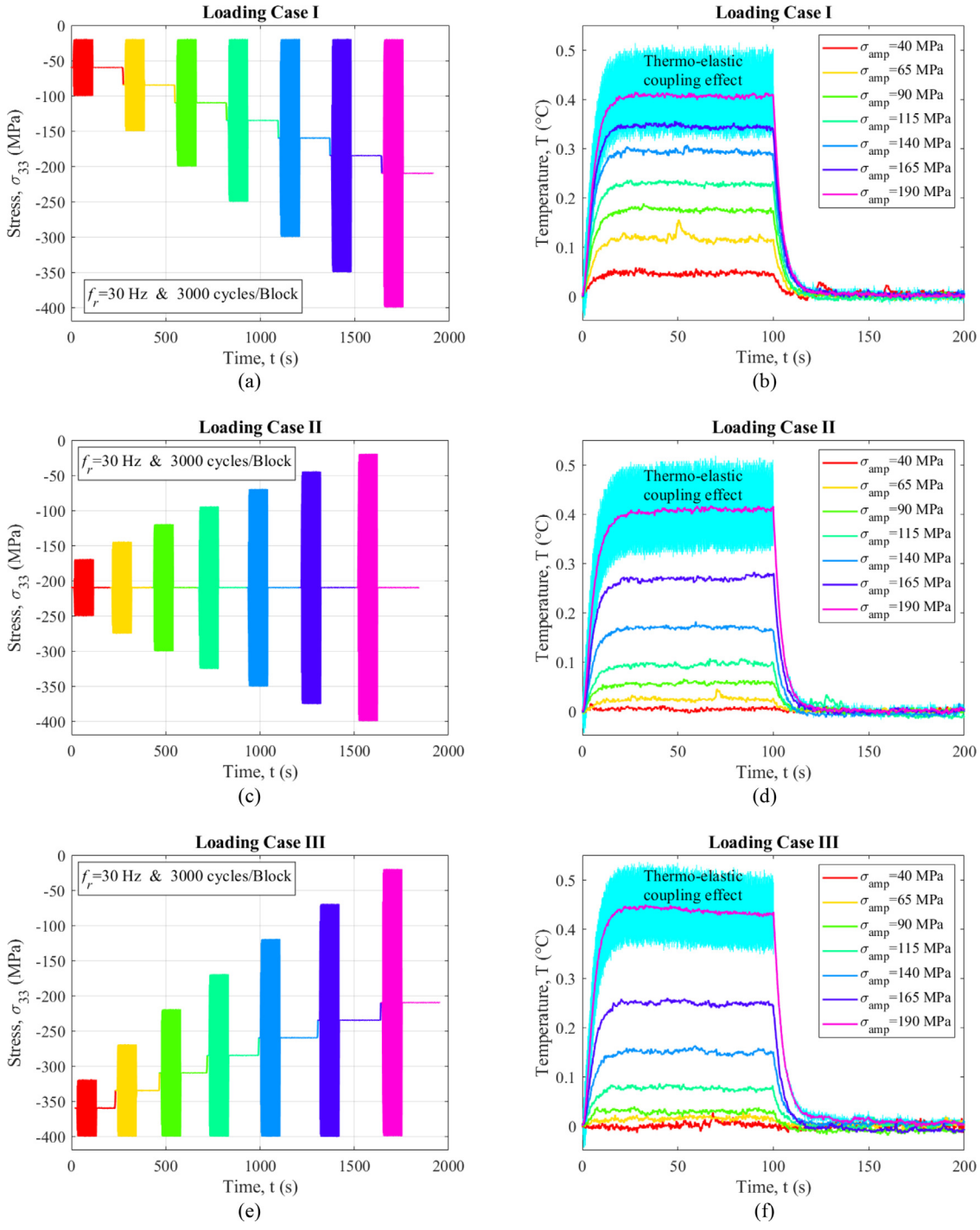

Fig. 5. Loading case I, II and III performed on non-polarized specimen (a, c and e) applied compressive stress versus time (b, d and f) temperature evolution during seven loading blocks with different stress amplitude (the cyan curve shows the temperature elevation at stress amplitude of 190 MPa, including fluctuations due to thermo-elastic coupling effect).

cases (i.e., the compressive stress varies between -20 and -400 MPa in the last loading block), which is not the case for other loading blocks. Stress variations during first loading block of these three loading cases are shown in Fig. 4. For loading cases II and III, the first loading block of the self-heating test is in a reasonably linear part of the stress-strain curve. On the contrary, for the loading case I, the first loading block of the self-heating test is in a significantly nonlinear part of the stress-strain curve (this nonlinearity implies more dissipative phenomena (i.e., domain switching) which occurs at stress levels lower than 150 MPa). It can be generalized to other loading blocks. Therefore, it will be expected that the internal dissipative energy in loading case I is more than that in loading cases II and III.

Stress variations in loading cases I, II and III as well as corresponding temperature evolutions of non-polarized specimens during their seven loading blocks are shown in Fig. 5.

As is shown in Fig. 5b, d and f, the temperature increases rapidly at the beginning of each loading block (during the first 600 cycles) and then it tends to reach a stationary value. The temperature stabilization correlates with a constant dissipated ther-

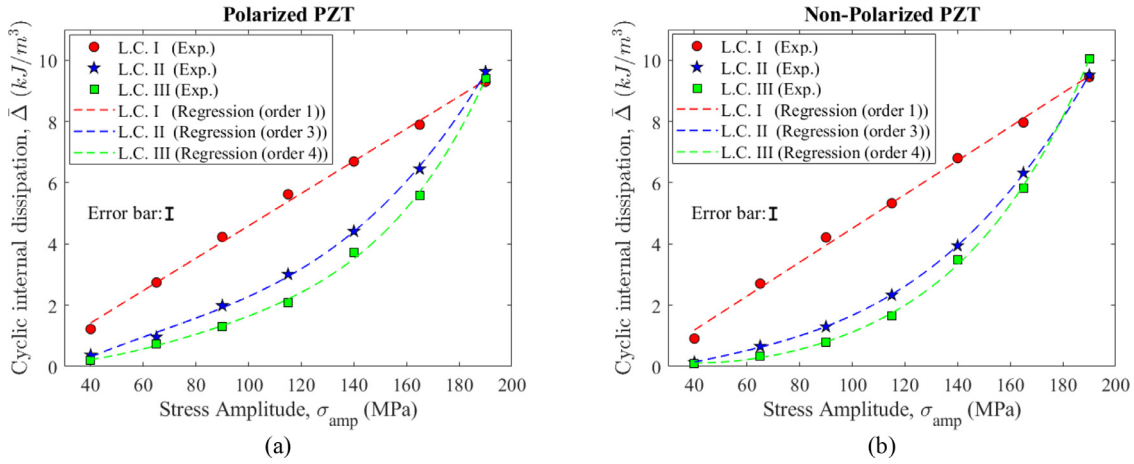

Fig. 6. Evolution of the cyclic internal dissipation as a function of the stress amplitude for (a) polarized and (b) non-polarized PZT specimens by applying loading cases I, II and III.

mal source. It implies a thermodynamic equilibrium between the energy induced by mechanical loading and the heat losses with the surroundings. The higher stress amplitudes lead to the higher mean steady state temperature following the same trend until it reaches about 0.4 °C for a stress amplitude of 190 MPa. It is worth noting that the reproducibility of the results was confirmed by performing three self-heating tests on the polarized specimens under loading case I.

To provide a comparable analysis, self-heating tests with above loading cases are also performed on polarized specimens. Then, for both polarized and non-polarized samples, the cyclic internal dissipation (or the internal dissipation per cycle, $\bar{\Delta}$) is evaluated for each loading block using Eq. (5). Fig. 6a and b present the cyclic internal dissipation versus the stress amplitude curves obtained for the polarized and non-polarized PZT specimens, respectively. These results highlight that the cyclic internal dissipation is evolving almost linearly with the stress amplitude during loading case I and is evolving nonlinearly with the stress amplitude during loading cases II and III. As it was expected, in the first loading block, the cyclic internal dissipation is close to zero for the loading cases II and III, while it is not zero for the loading case I. It is also worth noting that the last loading block does indeed provide identical results (as expected) for the three loading cases and allows an estimation of the error bar on the internal dissipation per cycle ($\bar{\Delta}$) around 0.19 kJ/m^3.

4. Polarization measurements under compression cyclic loading

This section describes the behavior of the polarized and non-polarized PZT ceramics subjected to cyclic compressive mechanical loading under low frequency ($f_r = 50\,mHz$). At such a low frequency, the released heat due to internal dissipation has enough time to transfer out completely and therefore the temperature of the specimen does not evolve significantly. On the other hand, it permits the measurement of stress-strain hysteresis loop area via DIC. The hysteresis loop area ($\int_{cycle} \boldsymbol{\sigma} : d\boldsymbol{\varepsilon}^{nl}$) provides a valuable information to evaluate energy dissipated upon cycling
($\overline{\Delta} = \int_{cycle} \boldsymbol{\sigma} : d\boldsymbol{\varepsilon}^{nl} - \int_{cycle} A_k : dV_k$) and it can be regarded as an indicator to study dissipative phenomena.

The same loading cases, as those considered to realize self-heating tests in Section 3.2, are considered to investigate further the hysteretic behavior during loading–unloading cycles. For the sake of stable closed hysteresis loop, five cycles are performed at each loading block, as shown in Fig. 7, and the results of the last cycle are used to evaluate hysteresis areas corresponding to each loading case. After the fourth cycle, the hysteresis loop area (i.e., the area enclosed by the loop) does not considerably vary from one cycle to the next one, and its fractional change is negligible. It should be pointed out that the hysteresis loop could be displaced slightly with each cycle. However, the shift of the hysteresis loop is not considered because, in this study, our interest is in the area enclosed by the hysteresis loop and not in its real position along the stress-strain or the stress-polarization curves.

As an example, evolution of stress-polarization and stress-strain hysteresis loops of the fifth cycle of each block during loading case I are shown in Fig. 8. In the following, the hysteresis loop area will be used to study the dissipated energy during above-mentioned three loading cases. It is worth mentioning that the hysteresis loop area gained from each pair of conjugate variables (e.g., stress-strain and polarization-electric field) is an energy quantity. While the hysteresis loop area acquired from the polarization-stress curve (Fig. 8a) is not an energy quantity, but corresponding information can be used as an insight to study the dissipated energy.

Fig. 9 shows the evolution of hysteresis areas versus the stress amplitude obtained for the polarized and non-polarized PZT specimens. To check the reproducibility of measurements, each loading case is repeated at least three times.

It is worth noting that polarization does not vary upon compressive mechanical loading in non-polarized PZT samples. Hence, in Fig. 9c, only the evolution of stress-strain hysteresis areas in non-polarized PZT samples is brought.

5. Discussion

The dissipation measured in this study is interpreted as resulting mostly from domain switching. Other sources of dissipation, however, could be considered. For instance, the electromechanical behavior of soft PZT ceramics can be accompanied by a structural phase transformation [73–75]. DIC technique can indirectly give access to this information through the material volume change [47,54]. Since the domain switching is an isochoric mechanism, the material volume variation is ascribed to other non-isochoric mechanisms such as elasticity, piezoelectricity and possible phenomena such as phase transformation or crack propagation. Regarding the experiments performed in this study, the observed volume change - although rather noisy due to the uncertainties on the transverse strain measurement - cannot be fully explained by elastic effects. A structural phase transformation is therefore suspected. Such a phase transformation could contribute to the temperature change of the samples. This contribution, however, was assumed to be small compared to the effect of domain switching. Some mechan-

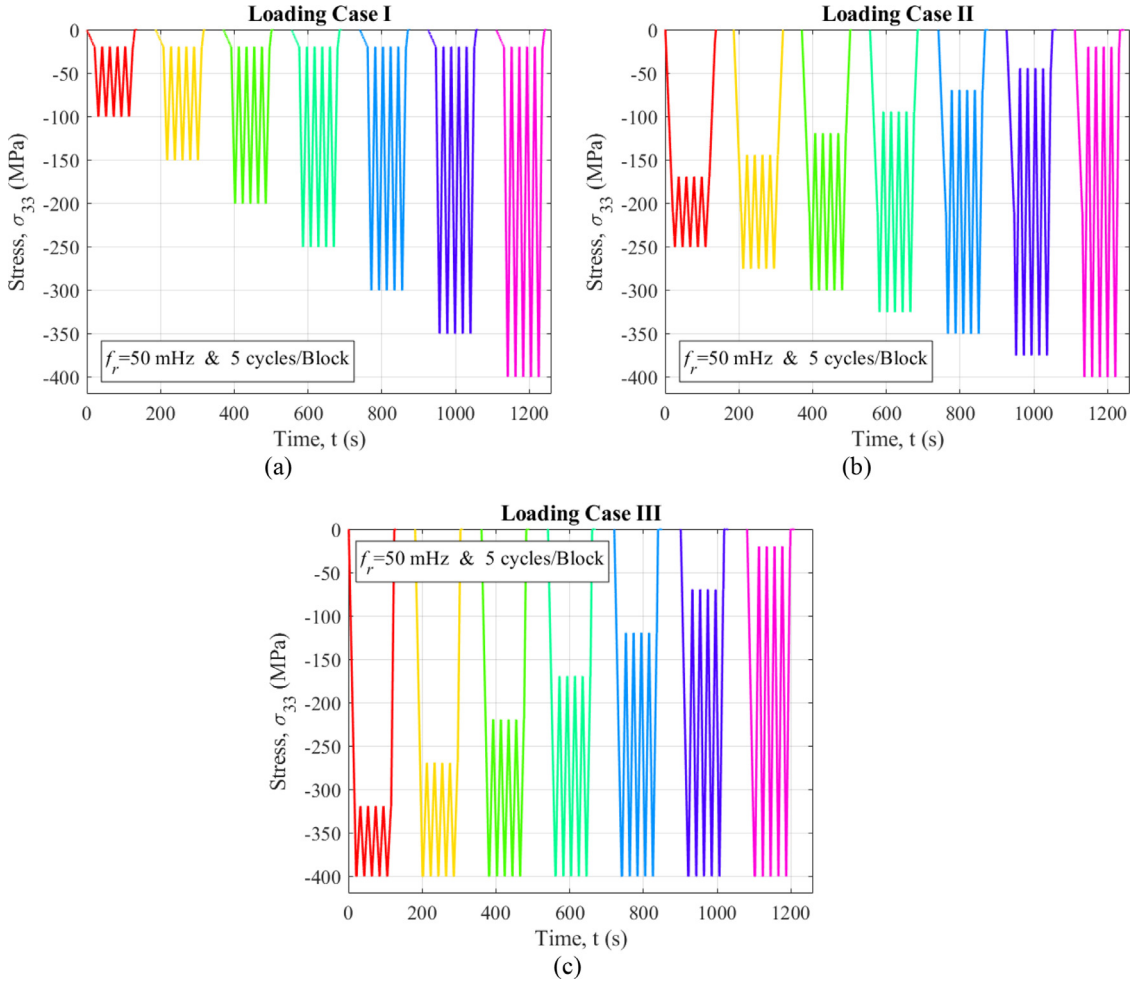

Fig. 7. Applied compressive stress versus time during compressive quasi-static ($f_r = 50\,mHz$) tests (a) loading case I (b) loading case II (c) loading case III.

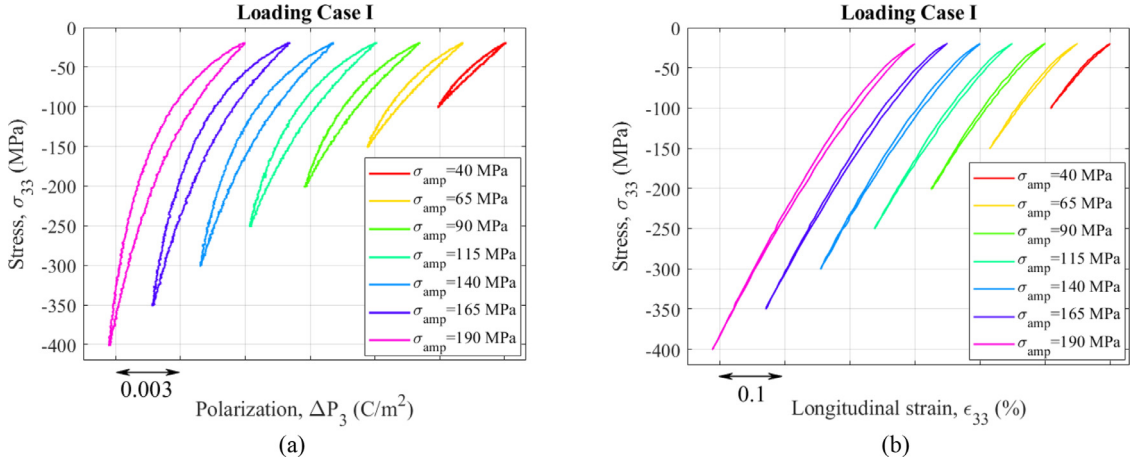

Fig. 8. (a) Stress-polarization and (b) stress-strain hysteresis loops for different stress amplitudes in loading case I obtained from polarized PZT sample.

ical degradation mechanisms, such as microcracking, can also be a source of internal dissipation [40,76]. Here, due to the moderate level of applied loadings, in terms of amplitude and number of cycles, no mechanical degradation has been observed in the tested samples. This possible source of dissipation will be neglected in the following. Therefore, in this study, the observed dissipation will be ascribed to domain switching.

All results obtained from DIC measurements under compressive cyclic loading at low frequency ($f_r = 50\,mHz$) and self-heating tests performed at frequency of 30 Hz are gathered in Fig. 10. For the sake of clarity, only regression curves are plotted in Fig. 10 which summarizes whole experimental data. Very similar trend is seen for variations of stress-strain hysteresis area and cyclic internal dissipation under considered three loading cases.

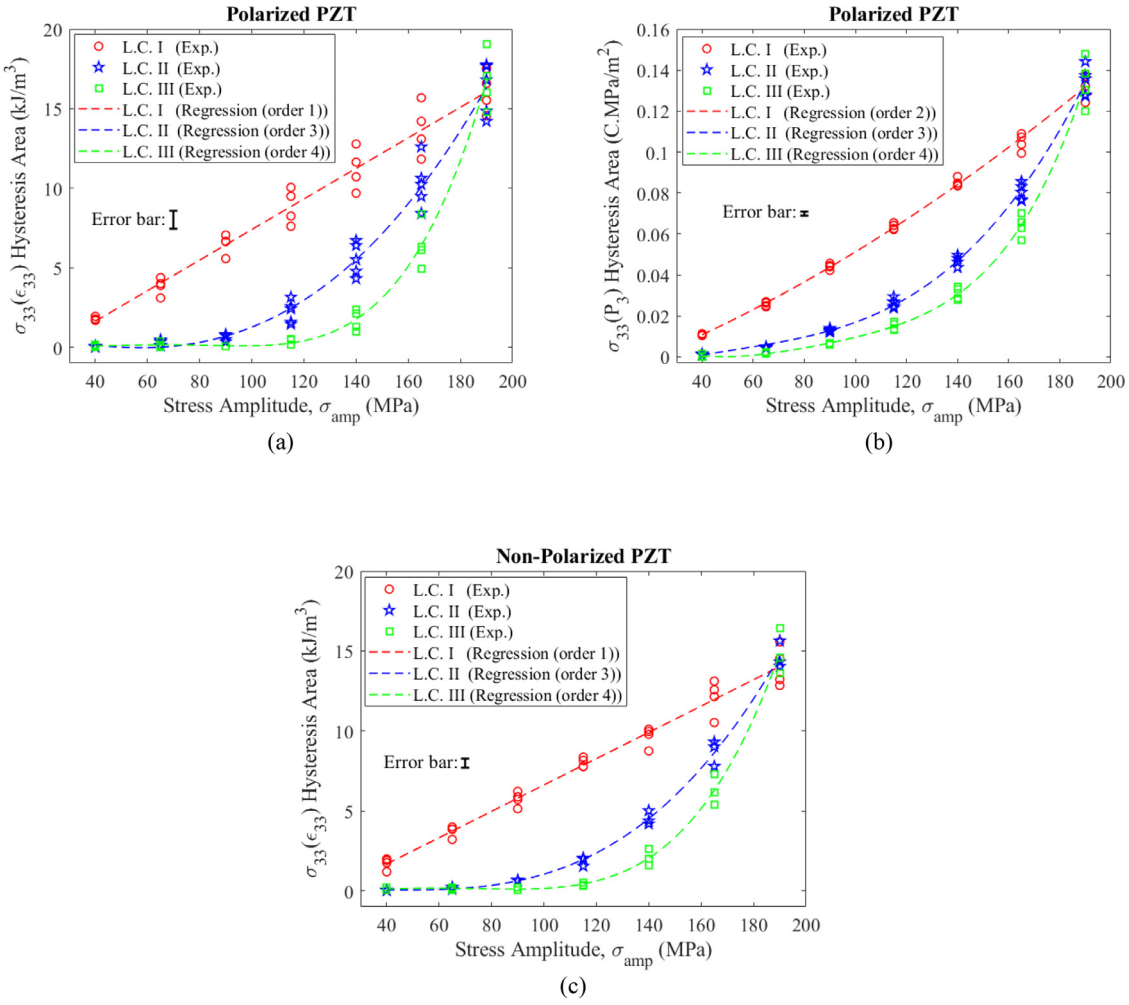

Fig. 9. Polarized PZT evolution of (a) stress-strain and (b) stress-polarization hysteresis areas versus stress amplitude and (c) non-polarized PZT evolution of stress-strain hysteresis areas versus stress amplitude.

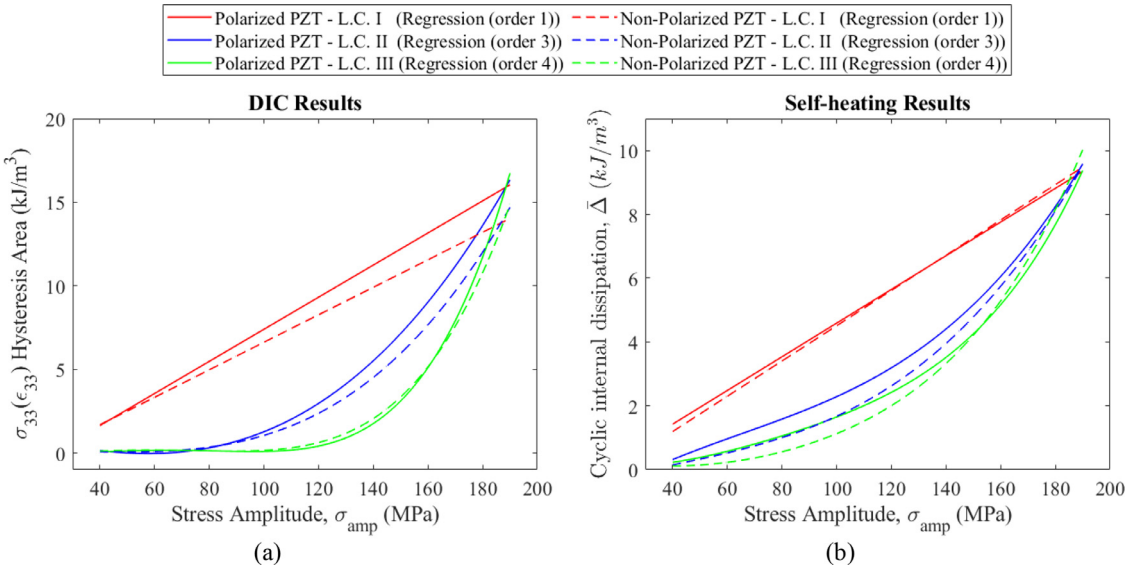

Fig. 10. Evolution of (a) stress-strain hysteresis area and (b) cyclic internal dissipation as a function of the stress amplitude for both polarized (plain lines) and non-polarized (dash lines) PZT specimens upon loading cases I, II and III (regression on experimental results obtained from DIC measurements (a) and self-heating tests(b)).

According to Fig. 10, case I is found to possess higher values of energy dissipation compared to cases II and III (exhibiting less dissipation under compressive mechanical cyclic loading). Variation of stress in loading case I covers more of the nonlinear part of the stress-strain curve (stress range of -20 up to -150 MPa in Fig. 4) where the effect of dissipative phenomena (i.e., domain switching) on the material behavior is presumably increased.

The obtained results from both DIC and self-heating measurements show that more dissipation is observed at low stress values. It implies that micro non-180 ° domain walls mobility is favored at low stress values (lower than 150 MPa). These results, consistently with previous observations, can also be interpreted as the existence of an enhanced electromechanical coupling at low stress levels which leads to more energy dissipation. At high stress amplitudes (more than 150 MPa), applied mechanical load reduces the domain wall contributions to the energy dissipation but energy dissipation is still observed. Therefore, it can be concluded that even in the macroscopically linear part of the stress-strain curve, domain switching occurs and contributes to energy dissipation upon mechanical cyclic loading. This conclusion is in line with the results of local investigation in the literature (e.g., [39]).

Other important point which can be drawn from Fig. 10 is that the initial state of the material (polarized or non-polarized) has little impact on the internal dissipation upon mechanical cyclic loading. These dissipative mechanisms are connected to non-180 ° domain switching generated by the application of the stress. Due to the application of a compressive stress of 400 MPa amplitude prior to the self-heating tests, the initial polarization state of the specimens is modified. The level of applied stress seems sufficient to make the domain states of all samples similar. Therefore, the non-180 ° domain switching generated during self-heating tests appear in similar proportions whatever the initial polarization level. The effect of the initial state of the material is only highlighted in the hysteresis area of the stress-strain curves at high stress amplitudes (Fig. 10a)).

For polarized material, the results of self-heating, DIC and polarization measurements represent almost the same trend which can be interpreted as a signature of domain wall activity. Polarization measurement is the easiest experimental procedure among them. However, this measurement procedure is not accessible for non-polarized material.

Since the frequency of the tests for DIC and self-heating measurements is different, the contribution of other state functions of conjugate variables ($\int_{cycle} A_k : dV_k$) to energy dissipated upon cycling ($\overline{\Delta} = \int_{cycle} \boldsymbol{\sigma} : d\boldsymbol{\varepsilon}^{nl} - \int_{cycle} A_k : dV_k$) cannot be determined explicitly. On the other hand, due to the limitation of acquisition frequency of DIC camera (maximum frame rate of 5 Hz), it was not possible to evaluate the effect of frequency on DIC measurement results. However, even without knowing the exact effect of frequency, one may conclude that the contribution of other state functions of conjugate variables ($\int_{cycle} A_k : dV_k$) to the total energy dissipated upon cycling ($\overline{\Delta}$) is considerable. Nevertheless, these results can be employed to propose a thermodynamic framework for investigating the dissipative phenomena under cyclic ferroelastic loadings.

The realized work robustly illustrates the capability of employed full-field methodologies (DIC and self-heating measurements) to quantify the dissipated energy of studied material upon compressive mechanical cyclic loading, even when the materials are non-polarized. This study represents a first step toward the investigation of dissipative mechanisms upon mechanical cyclic loadings (i.e., ferroelastic cyclic behavior). Future work will concentrate on proposing a model based on the thermodynamics of irreversible processes, to reproduce the obtained self-heating results.

6. Conclusion

In this paper self-heating and dissipative effects in soft PZT ceramics are studied under compressive cyclic mechanical loadings. Cyclic mechanical loadings are applied on polarized and non-polarized PZT specimens by considering three loading patterns. DIC and self-heating measurements are employed to quantify dissipated energy in the studied material under the considered mechanical loadings. This study sheds new light on dissipative mechanisms occurring during cyclic ferroelastic loadings and enables the magnitude of non-linear mechanisms to be quantified. The origin of nonlinearities observed during the considered mechanical loadings is attributed to non-180 ° domain switching which is shown to be more pronounced at low stress levels. For polarized specimens, the results of self-heating, DIC and polarization measurements follow the same trend which can be interpreted as a signature of domain wall activity. Polarization measurement is the easiest experimental procedure. However, the hysteresis loop area obtained from the polarization-stress curves is not an energy quantity, and this measurement procedure is not accessible for non-polarized material. On the other hand, it is not a straightforward task to perform self-heating test on PZT specimen subjected to mechanical cyclic loadings. It is also shown that, due to the compressive stress experienced by all specimens prior to self-heating measurements, the initial state of the material (polarized or non-polarized) has a negligible impact, for the studied material, on the internal dissipation upon mechanical cyclic loadings.

Declaration of Competing Interest

None.

Supplementary materials

Supplementary material associated with this article can be found, in the online version, at doi:10.1016/j.actamat.2021.117386.

References

[1] W. Heywang, K. Lubitz, W. Wersing, Piezoelectricity, Springer, Berlin, Heidelberg, 2008 Berlin Heidelberg, doi:10.1007/978-3-540-68683-5.
[2] D.C. Lupascu, J. Rödel, Fatigue in bulk lead zirconate titanate actuator materials, Adv. Eng. Mater. 7 (2005) 882–898, doi:10.1002/adem.200500117.
[3] Q.M. Zhang, H. Wang, N. Kim, L.E. Cross, Direct evaluation of domain-wall and intrinsic contributions to the dielectric and piezoelectric response and their temperature dependence on lead zirconate-titanate ceramics, J. Appl. Phys. 75 (1994) 454–459, doi:10.1063/1.355874.
[4] D. Damjanovic, Contributions to the piezoelectric effect in ferroelectric single crystals and ceramics, J. Am. Ceram. Soc. 88 (2005) 2663–2676, doi:10.1111/j.1551-2916.2005.00671.x.
[5] D. Damjanovic, Hysteresis in piezoelectric and ferroelectric materials, in: The Science Hysteresis, Academic Press, 2006, pp. 337–465, doi:10.1016/B978-012480874-4/50022-1.
[6] H. Cao, A.G. Evans, Nonlinear deformation of ferroelectric ceramics, J. Am. Ceram. Soc. 76 (1993) 890–896, doi:10.1111/j.1151-2916.1993.tb05312.x.
[7] M. Kamlah, Ferroelectric and ferroelastic piezoceramics - modeling of electromechanical hysteresis phenomena, Contin. Mech. Thermodyn. 13 (2001) 219–268, doi:10.1007/s001610100052.
[8] B. Jaffe, W.R. Cook, H.L. Jaffe, Piezoelectric Ceramics, Academic Press, 1971.
[9] D.A. Hall, Nonlinearity in piezoelectric ceramics, J. Mater. Sci. 36 (2001) 4575–4601, doi:10.1023/A:1017959111402.
[10] S. Li, W. Cao, L.E. Cross, The extrinsic nature of nonlinear behavior observed in lead zirconate titanate ferroelectric ceramic, J. Appl. Phys. 69 (1991) 7219–7224, doi:10.1063/1.347616.
[11] G. Liu, S. Zhang, W. Jiang, W. Cao, Losses in ferroelectric materials, Mater. Sci. Eng. R Rep. 89 (2015) 1–48, doi:10.1016/j.mser.2015.01.002.
[12] D. Damjanovic, M. Demartin, Contribution of the irreversible displacement of domain walls to the piezoelectric effect in barium titanate and lead zirconate titanate ceramics, J. Phys. Condens. Matter. 9 (1997) 4943–4953, doi:10.1088/0953-8984/9/23/018.
[13] B. Jaffe, R.S. Roth, S. Marzullo, Properties of piezoelectric ceramics in the solid-solution series lead titanate-lead zirconate-lead oxide: tin oxide and lead titanate-lead hafnate, J. Res. Natl. Bur. Stand. 55 (1955) (1934) 239, doi:10.6028/jres.055.028.

[14] K. Uchino, S. Hirose, Loss mechanisms in piezoelectrics: how to measure different losses separately, IEEE Trans. Ultrason. Ferroelectr. Freq. Control 48 (2001) 307–321, doi:10.1109/58.896144.
[15] J. Glaum, T. Granzow, L.A. Schmitt, H.J. Kleebe, J. Rödel, Temperature and driving field dependence of fatigue processes in PZT bulk ceramics, Acta Mater. 59 (2011) 6083–6092, doi:10.1016/j.actamat.2011.06.017.
[16] A. Martin, K. Kakimoto, K. Hatano, Y. Doshida, Temperature dependence of unipolar fatigue behavior of lead-free alkali niobate ceramics, J. Ceram. Soc. Japan 124 (2016) 730–736, doi:10.2109/jcersj2.15279.
[17] C. Verdier, D. Lupascu, J. Rödel, Unipolar fatigue of ferroelectric lead–zirconate–titanate, J. Eur. Ceram. Soc. 23 (2003) 1409–1415, doi:10.1016/S0955-2219(02)00351-5.
[18] N. Balke, D.C. Lupascu, T. Granzow, J. Rödel, Fatigue of lead zirconate titanate ceramics. I: unipolar and DC loading, J. Am. Ceram. Soc. 90 (2007) 1081–1087, doi:10.1111/j.1551-2916.2007.01520.x.
[19] H. Wang, S.M. Lee, J.L. Wang, H.T. Lin, Fatigue of extracted lead zirconate titanate multilayer actuators under unipolar high field electric cycling, J. Appl. Phys. 116 (2014) 234101, doi:10.1063/1.4904352.
[20] Y. Zhang, J. Glaum, M.C. Ehmke, K.J. Bowman, J.E. Blendell, M.J. Hoffman, Unipolar fatigue behavior of BCTZ lead-free piezoelectric ceramics, J. Am. Ceram. Soc. 99 (2016) 1287–1293, doi:10.1111/jace.14103.
[21] M. Mitrovic, G. Carman, F. Straub, Durability characterization of piezoelectric stack actuators under combined electro-mechanical loading, in: Proceedings of the 41st Structures, Structural Dynamics, and Materials Conference and Exhibit, Reston, Virigina, American Institute of Aeronautics and Astronautics, 2000, pp. 217–232, doi:10.2514/6.2000-1500.
[22] V.C. Lo, W.W.Y. Chung, S.C.K. Chow, Electromechanical properties of ferroelectric thin films under alternating mechanical and electrical loadings, in: Proceedings of the Sixteenth IEEE International Symposium Applcation Ferroelectrics, IEEE, 2007, pp. 728–731, doi:10.1109/ISAF.2007.4393384.
[23] N. Balke, D.C. Lupascu, T. Granzow, J. Rödel, Fatigue of lead zirconate titanate ceramics II: sesquipolar loading, J. Am. Ceram. Soc. 90 (2007) 1088–1093, doi:10.1111/j.1551-2916.2007.01521.x.
[24] L. Yingwei, C. Xiangyang, Z. Dapeng, G. Zhipeng, Influence of domain switching process on the electrical fatigue behavior of ferroelectrics, Ceram. Int. 46 (2020) 24213–24224, doi:10.1016/j.ceramint.2020.06.201.
[25] S. Zhukov, J. Glaum, H. Kungl, E. Sapper, R. Dittmer, Y.A. Genenko, H. Von Seggern, Fatigue effect on polarization switching dynamics in polycrystalline bulk ferroelectrics, J. Appl. Phys. (2016) 120, doi:10.1063/1.4960691.
[26] Y. Mohan, A. Arockiarajan, Experimental and theoretical investigation of temperature-dependent electrical fatigue studies on 1-3 type piezocomposites, AIP Adv. 6 (2016), doi:10.1063/1.4944582.
[27] Y. Zhang, J. Glaum, M.C. Ehmke, J.E. Blendell, K.J. Bowman, M.J. Hoffman, High bipolar fatigue resistance of BCTZ lead-free piezoelectric ceramics, J. Am. Ceram. Soc. 99 (2016) 174–182, doi:10.1111/jace.13927.
[28] F.J. Yang, X. Cheng, Y. Zhang, An *in-situ* Raman spectroscopic investigation in electric fatigue behaviors of PLZT ceramics, Ceram. Int. 42 (2016) 2324–2329, doi:10.1016/j.ceramint.2015.10.028.
[29] A. Mazzalai, D. Balma, N. Chidambaram, R. Matloub, P. Muralt, Characterization and fatigue of the converse piezoelectric effect in PZT films for MEMS applications, J. Microelectromechanical Syst. 24 (2015) 831–838, doi:10.1109/JMEMS.2014.2353855.
[30] M. Hinterstein, J. Rouquette, J. Haines, P. Papet, J. Glaum, M. Knapp, J. Eckert, M. Hoffman, Structural contribution to the ferroelectric fatigue in lead zirconate titanate ceramics, Phys. Rev. BCover. Condens. Matter Mater. Phys. 90 (2014) 1–7, doi:10.1103/PhysRevB.90.094113.
[31] F.Z. Yao, E.A. Patterson, K. Wang, W. Jo, J. Rödel, J.F. Li, Enhanced bipolar fatigue resistance in CaZrO3-modified (K,Na)NbO3 lead-free piezoceramics, Appl. Phys. Lett. 104 (2014) 3–8, doi:10.1063/1.4884826.
[32] J. Glaum, M. Hoffman, Electric fatigue of lead-free piezoelectric materials, J. Am. Ceram. Soc. 97 (2014) 665–680, doi:10.1111/jace.12811.
[33] Z. Fan, J. Koruza, J. Rödel, X. Tan, An ideal amplitude window against electric fatigue in BaTiO3-based lead-free piezoelectric materials, Acta Mater. 151 (2018) 253–259, doi:10.1016/j.actamat.2018.03.067.
[34] S. Pojprapai (Imlao), J.L. Jones, A.J. Studer, J. Russell, N. Valanoor, M. Hoffman, Ferroelastic domain switching fatigue in lead zirconate titanate ceramics, Acta Mater. 56 (2008) 1577–1587, doi:10.1016/j.actamat.2007.11.044.
[35] P.M. Chaplya, G.P. Carman, Compression of piezoelectric ceramic at constant electric field: energy absorption through non-180° domain-wall motion, J. Appl. Phys. 92 (2002) 1504–1510, doi:10.1063/1.1489498.
[36] J.M. Calderon-Moreno, M. Popa, Stress dependence of reversible and irreversible domain switching in PZT during cyclic loading, Mater. Sci. Eng. A 336 (2002) 124–128, doi:10.1016/S0921-5093(01)01976-1.
[37] J.M. Calderon Moreno, F. Guiu, M. Meredith, M.J. Reece, N.M.N. Alford, S.J. Penn, Anisotropic and cyclic mechanical properties of piezoelectrics - compression testing, J. Eur. Ceram. Soc. 19 (1999) 1321–1324, doi:10.1016/s0955-2219(98)00434-8.
[38] A. Pramanick, D. Damjanovic, J.E. Daniels, J.C. Nino, J.L. Jones, Origins of electro-mechanical coupling in polycrystalline ferroelectrics during subcoercive electrical loading, J. Am. Ceram. Soc. 94 (2011) 293–309, doi:10.1111/j.1551-2916.2010.04240.x.
[39] L. Daniel, D.A. Hall, J. Koruza, K.G. Webber, A. King, P.J. Withers, Revisiting the blocking force test on ferroelectric ceramics using high energy X-ray diffraction, J. Appl. Phys. 117 (2015) 174104, doi:10.1063/1.4918928.
[40] H.S. Chen, H.L. Wang, Y.M. Pei, Y.J. Wei, B. Liu, D.N. Fang, Crack instability of ferroelectric solids under alternative electric loading, J. Mech. Phys. Solids. 81 (2015) 75–90, doi:10.1016/j.jmps.2015.04.014.
[41] B. Amini, Y. Demmouche, M. Barati, G. Helbert, S.A. Chirani, S. Calloch, Self-heating of metastable 304L austenitic stainless steel under cyclic loading: influence of initial martensite volume fraction, testing temperature and pre-strain, Mech. Mater. 151 (2020) 103596, doi:10.1016/j.mechmat.2020.103596.
[42] L. Bercelli, S. Moyne, M. Dhondt, C. Doudard, S. Calloch, J. Beaudet, A probabilistic approach for high cycle fatigue of wire and arc additive manufactured parts taking into account process-induced pores, Addit. Manuf. 42 (2021) 101989, doi:10.1016/j.addma.2021.101989.
[43] P. Bayati, A. Jahadakbar, M. Barati, M. Nematollahi, L. Saint-Sulpice, M. Haghshenas, S.A. Chirani, M.J. Mahtabi, M. Elahinia, Toward low and high cycle fatigue behavior of SLM-fabricated NiTi: considering the effect of build orientation and employing a self-heating approach, Int. J. Mech. Sci. 185 (2020) 105878, doi:10.1016/j.ijmecsci.2020.105878.
[44] P. Mostofizadeh, M. Kadkhodaei, S. Arbab Chirani, L. Saint-Sulpice, M. Rokbani, T. Bouraoui, S. Calloch, Fatigue analysis of shape memory alloys by self-heating method, Int. J. Mech. Sci. 156 (2019) 329–341, doi:10.1016/j.ijmecsci.2019.04.012.
[45] M. Naderi, M.M. Khonsari, Thermodynamic analysis of fatigue failure in a composite laminate, Mech. Mater. 46 (2012) 113–122, doi:10.1016/j.mechmat.2011.12.003.
[46] M. Barati, F. Bahari-sambran, A. Saeedi, S.A. Chirani, R. Eslami-Farsanib, Fatigue properties determination of carbon fiber reinforced epoxy composite by self-heating measurements, in: Proceedings of the 24ème Congrès Français de Mécanique, 2019, pp. 1–11. https://cfm2019.sciencesconf.org/255103/document.
[47] V. Segouin, M. Domenjoud, Y. Bernard, L. Daniel, Electro-mechanical behavior of ferroelectrics: insights into local contributions from macroscopic measurements, Acta Mater. 211 (2021) 116870, doi:10.1016/j.actamat.2021.116870.
[48] V. Segouin, M. Domenjoud, Y. Bernard, L. Daniel, Development of a 2D DIC experimental tool for piezoelectric strains measurements, in: Proceedings of the Society for Experimental Mechanics Conference, Springer New York LLC, 2017, pp. 45–50, doi:10.1007/978-3-319-51439-0_11.
[49] V. Segouin, M. Domenjoud, Y. Bernard, L. Daniel, Mechanics-aided digital image correlation for the investigation of piezoelectric and ferroelectric behavior of a soft PZT, J. Eur. Ceram. Soc. 39 (2019) 2091–2102, doi:10.1016/j.jeurceramsoc.2018.12.058.
[50] M.H. Malakooti, H.A. Sodano, Noncontact and simultaneous measurement of the d33 and d 31 piezoelectric strain coefficients, Appl. Phys. Lett. 102 (2013) 061901, doi:10.1063/1.4791573.
[51] M.H. Malakooti, H.A. Sodano, Direct measurement of piezoelectric shear coefficient, J. Appl. Phys. 113 (2013) 214106, doi:10.1063/1.4809636.
[52] D. Chen, M. Kamlah, Deformation in lead zirconate titanate ceramics under large signal electric field loading measured by digital image correlation, Rev. Sci. Instrum. 86 (2015) 113707, doi:10.1063/1.4936353.
[53] D. Chen, E. Carter, M. Kamlah, Deformation behavior of lead zirconate titanate ceramics under uniaxial compression measured by the digital image correlation method, Smart Mater. Struct. 25 (2016) 097001, doi:10.1088/0964-1726/25/9/097001.
[54] S. Venkateshwarlu, L.K. Venkataraman, V. Segouin, F.P. Marlton, H.C. Hin, D. Chernyshov, Y. Ren, M.R.V. Jørgensen, S. Nayak, J. Rödel, L. Daniel, A. Pramanick, Large electromechanical strain and unconventional domain switching near phase convergence in a Pb-free ferroelectric, Commun. Phys. 3 (2020) 193, doi:10.1038/s42005-020-00459-2.
[55] H. Sen Chen, Y.M. Pei, B. Liu, D.N. Fang, Rate dependant heat generation in single cycle of domain switching of lead zirconate titanate via in-situ spontaneous temperature measurement, Appl. Phys. Lett. 102 (2013) 242912, doi:10.1063/1.4811702.
[56] J. Wang, T. Yang, K. Wei, X. Yao, Temperature-electric field hysteresis loop of electrocaloric effect in ferroelectricity-direct measurement and analysis of electrocaloric effect. i, Appl. Phys. Lett. 102 (2013) 152907, doi:10.1063/1.4801997.
[57] O.V. Malyshkina, A.Y. Eliseev, R.M. Grechishkin, Dispersion of switching processes in ferroelectric ceramics, Adv. Condens. Matter Phys. 2017 (2017) 1–5, doi:10.1155/2017/2507808.
[58] A. Grünebohm, Y.B. Ma, M. Marathe, B.X. Xu, K. Albe, C. Kalcher, K.C. Meyer, V.V. Shvartsman, D.C. Lupascu, C. Ederer, Origins of the inverse electrocaloric effect, Energy Technol. 6 (2018) 1491–1511, doi:10.1002/ente.201800166.
[59] M. Wingen, A. Ricoeur, Caloric aspects of nonlinear ferroelectric constitutive behavior: modeling and simulation, Contin. Mech. Thermodyn. 31 (2019) 549–568, doi:10.1007/s00161-018-0711-1.
[60] O. El Khatib, S. Kozinov, M. Kuna, A micro–macro scale approach for thermal effects in ferroelectrics, Contin. Mech. Thermodyn. 31 (2019) 1439–1452, doi:10.1007/s00161-019-00760-8.
[61] F. Wang, T. Liu, C.L. Xie, Y. Liu, N.S. Ma, J. Duan, J.R. He, B. Li, B.L. Ou, Y. Ou, J.J. Cheng, Q. Liu, L.F. Liu, W. Wang, Temperature-electric field hysteresis loop of multicaloric effects in PbZr0.8Ti0.2O3 thin films, Phys. Lett. A 383 (2019) 2933–2937, doi:10.1016/j.physleta.2019.06.033.
[62] A. Bradeško, A. Hedl, L. Fulanović, N. Novak, T. Rojac, Self-heating of relaxor and ferroelectric ceramics during electrocaloric field cycling, APL Mater. 7 (2019) 071111, doi:10.1063/1.5109028.
[63] A. Warkentin, A. Ricoeur, A semi-analytical scale bridging approach towards polycrystalline ferroelectrics with mutual nonlinear caloric-electromechanical

couplings, Int. J. Solids Struct. 200–201 (2020) 286–296, doi:10.1016/j.ijsolstr.2020.05.016.
[64] S. Cang, J. Chen, C. Lu, Evolution of the electrical displacement and energy dissipation of lead zirconate-titanate ceramics under cyclical load, Adv. Mater. Sci. Eng. 2020 (2020) 1–12, doi:10.1155/2020/6975968.
[65] M. Stewart, M.G. Cain, D. Hall, Ferroelectric hysteresis measurement & analysis, NPL Rep. CMMT (1999) 1–57 http://www.opengrey.eu/item/display/10068/677928.
[66] A.M. Glazer, P. Groves, D.T. Smith, Automatic sampling circuit for ferroelectric hysteresis loops, J. Phys. E 17 (1984) 95–97, doi:10.1088/0022-3735/17/2/001.
[67] Z. Tomičevć, F. Hild, S. Roux, Mechanics-aided digital image correlation, J. Strain Anal. Eng. Des. 48 (2013) 330–343, doi:10.1177/0309324713482457.
[68] D. Zhou, M. Kamlah, D. Munz, Effects of bias electric fields on the non-linear ferroelastic behavior of soft lead zirconate titanate piezoceramics, J. Am. Ceram. Soc. 88 (2005) 867–874, doi:10.1111/j.1551-2916.2005.00139.x.
[69] K.G. Webber, E. Aulbach, T. Key, M. Marsilius, T. Granzow, J. Rödel, Temperature-dependent ferroelastic switching of soft lead zirconate titanate, Acta Mater. 57 (2009) 4614–4623, doi:10.1016/j.actamat.2009.06.037.
[70] J. Fan, W.A. Stoll, C.S. Lynch, Nonlinear constitutive behavior of soft and hard PZT: experiments and modeling, Acta Mater. 47 (1999) 4415–4425, doi:10.1016/S1359-6454(99)00306-7.
[71] Noliac A/S, CTS Company, http://www.noliac.com, Hejreskovvej 18, DK-3490 Kvistgaard, Denmark.
[72] A. Chrysochoos, H. Louche, An infrared image processing to analyze the calorific effects accompanying strain localisation, Int. J. Eng. Sci. 38 (2000) 1759–1788, doi:10.1016/S0020-7225(00)00002-1.
[73] G. Esteves, C.M. Fancher, S. Röhrig, G.A. Maier, J.L. Jones, M. Deluca, Electric-field-induced structural changes in multilayer piezoelectric actuators during electrical and mechanical loading, Acta Mater. 132 (2017) 96–105, doi:10.1016/j.actamat.2017.04.014.
[74] Y.H. Seo, D.J. Franzbach, J. Koruza, A. Benčan, B. Malič, M. Kosec, J.L. Jones, K.G. Webber, Nonlinear stress-strain behavior and stress-induced phase transitions in soft Pb(Zr 1−x Tix)O 3 at the morphotropic phase boundary, Phys. Rev. B 87 (2013) 094116, doi:10.1103/PhysRevB.87.094116.
[75] M. Hinterstein, J. Rouquette, J. Haines, P. Papet, M. Knapp, J. Glaum, H. Fuess, Structural description of the macroscopic piezo- and ferroelectric properties of lead zirconate titanate, Phys. Rev. Lett. 107 (2011) 077602, doi:10.1103/PhysRevLett.107.077602.
[76] I. Westram, W.S. Oates, D.C. Lupascu, J. Rödel, C.S. Lynch, Mechanism of electric fatigue crack growth in lead zirconate titanate, Acta Mater. 55 (2007) 301–312, doi:10.1016/j.actamat.2006.08.029.